JOURNAL OF SPACECRAFT AND ROCKETS
Vol. 32, No. 1, January–February 1995

Whipple Shields Characterized by a Nondimensional Geometry Parameter

Kevin R. Housen* and Robert M. Schmidt†
Boeing Defense and Space Group, Seattle, Washington 98124

Impacts onto single-bumper (Whipple) shields were conducted using a technique that allows simulation of aluminum impacts onto aluminum shields at velocities up to 21 km/s. The results provided information on how the threshold impactor diameter for incipient perforation of the wall depends on the thickness b of the bumper, the thickness t of the spacecraft wall, and the spacing S between the bumper and the wall. Experiments were conducted to test a scaling prediction that these three variables are described by a single nondimensional parameter, $\pi_t = tS^2/b^3$, for aluminum impacts faster than 7 km/s. Experiments at simulated velocities near 10 and 17 km/s confirmed the prediction. Additional tests revealed the effects of π_t on the ballistic limit curve, which expresses the threshold diameter for perforation as a function of impact velocity. For velocities above about 10 km/s, the ballistic limit curve is nearly flat if π_t is less than a few thousand, and has a positive slope for larger values. This result, which differs significantly from existing ballistic limit models, is believed to be due to fractional vaporization of the impactor and bumper at high velocities. An empirical expression was developed that can be used to calculate the threshold impactor diameter as a function of t, S, and b for impact velocities up to 18 km/s.

Nomenclature

A, B, C	= parameters in ballistic limit equation
b	= thickness of bumper
d	= diameter of smallest impactor capable of perforating the wall
h_i	= energy per unit mass for melting of impactor
S	= spacing between bumper and wall
t	= thickness of wall
U	= impactor velocity
θ	= angle of impact (from normal)
π_t	= tS^2/b^3, nondimensional geometry parameter
ϕ	= a power-law exponent

Introduction

SPACECRAFT designers are faced with the challenge of shielding against meteoroid and orbital-debris impacts. Although several types of debris shields have been proposed, the simplest is the so-called Whipple shield, which consists of a single bumper, i.e., a flat sheet, positioned in front of the spacecraft wall. The purpose of the bumper is to fragment, melt or vaporize an impacting particle, thereby spreading the loading on the spacecraft wall over as large an area as possible.

One of the major problems in shield design is to determine whether a shield can prevent a given impact from perforating the wall. Typically, this question has been addressed through experiments for impacts at velocities below about 7 km/s and through model estimates at higher velocities, where practical constraints currently preclude launching spherical or chunky particles. Although several models of the high-velocity response of Whipple shields have been described in the literature, differences among these relationships, and the inability to verify them experimentally, have resulted in significant uncertainty in shield effectiveness at velocities above 7 km/s. To remedy this problem, techniques have been developed[1–4] that allow tests conducted at velocities below 7 km/s to simulate the relevant physical mechanisms[5] that occur in higher-velocity impacts. In such a simulation, the material of interest, i.e., the prototype material, is replaced by a surrogate that melts and vaporizes at lower impact velocities than does the prototype. For example, Hopkins et al.[5] used cadmium impactors and bumpers to simulate the effects of melting and vaporization that should occur in higher-speed impacts on more common structural metals, such as aluminum. They showed that the minimum wall thickness required to prevent perforation alternately increases and decreases as impact velocity is increased. They explained this behavior by noting that the minima and maxima are located at the velocities where impactor shattering, melting, and vaporization occur. The shape of the curve of wall thickness vs velocity for cadmium was shown to be similar to the curve for aluminum, except that the shattering, melting, and vaporization features occurred at lower velocities for cadmium, as expected in view of its relatively low heats of fusion and vaporization. In another surrogate-material study, Mullin et al.[2] reported results for impacts onto Whipple shields that showed the momentum delivered to the wall by the debris cloud in prototype aluminum impacts was reproduced by reduced-velocity tests using zinc or cadmium as surrogates for the projectile and bumper.

More recently, Schmidt et al.[4] showed that cadmium is an excellent material for studying the high-velocity response of aluminum shields. The prototype, in which the impactor, bumper, and wall are composed of aluminum, was simulated by replacing the impactor and bumper with cadmium surrogates having the same dimensions as the prototype. A scaling analysis showed that a cadmium sphere launched at velocity U duplicates a prototype impact at velocity $3.1U$ with regard to the degree of melting and vaporization in the debris cloud and the impulsive loading distribution on the wall. The velocity scale factor of 3.1 was shown to correlate the results of Hopkins et al.[5] for cadmium and aluminum. Additionally, Ref. 4 showed that cadmium tests at 2.3 km/s exhibited the same threshold impactor diameter for wall perforation as that found in prototype aluminum tests at 7 km/s (i.e. 3.1×2.3 km/s).

Reference 4 considered the case in which a structural failure of the wall results from the impact of the largely molten or vaporized debris cloud produced when a projectile strikes and penetrates the bumper. A model of wall failure was developed that showed perforation occurs when the specific impulse (momentum per unit area) delivered to the wall exceeds a critical value. The specific impulse was expressed in terms of the variables shown in Fig. 1. Using dimensional analysis, the functional relationship was simplified in terms of nondimensional ratios of the independent variables. Three conditions were imposed: 1) the impactor and bumper are composed of like materials (e.g., cadmium on cadmium, or aluminum on aluminum); 2) the wall material in the simulation is the same as in the prototype; and 3) all dimensions in the simulation are the same as in the prototype. This simplified the analysis because many of

Received Feb. 25, 1994; revision received Aug. 1, 1994; accepted for publication Aug. 22, 1994.

*Principal Engineer, Shock Physics, M/S 8H-05.
†Technical Fellow, Shock Physics, M/S 8H-05.

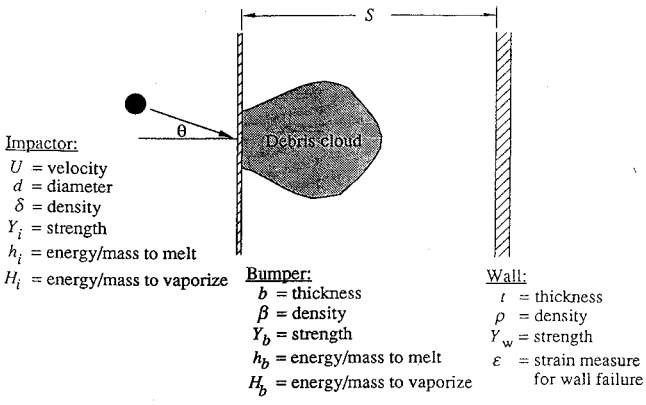

Fig. 1 Definition of variables used in analysis of Whipple shields.

the nondimensional parameters are constant under these conditions, and because terms involving ratios of material properties are constant when cadmium is used to simulate an aluminum impactor and bumper.

In addition to the above conditions, it was assumed that the specific impulse delivered to the wall is proportional to $1/S^2$. Justification of this assumption for the case of spherical impactors was presented in Ref. 4. However, distinctly nonspherical objects, such as disks, can produce debris clouds whose specific impulse does not vary as $1/S^2$ (and in fact may be nearly independent of S). Therefore, the present analysis is applied only to the case of spherical impactors.

The analysis in Ref. 4 resulted in the following expression for the diameter d of the smallest impactor able to perforate the wall:

$$\frac{d}{b} = f\left(\frac{U}{\sqrt{h_i}}, \theta, \frac{tS^2}{b^3}\right) \tag{1}$$

The first term on the right side is the scaled impact velocity, i.e., the actual impactor velocity divided by the square root of the heat of fusion of the impactor (and bumper) material. Simulations are conducted at the same scaled velocity as in the prototype. Therefore, the simulated aluminum impact velocity is $U_{Al} = (h_{i,Al}/h_{i,Cd})^{\frac{1}{2}} U_{Cd}$, where U_{Cd} is the actual velocity in the cadmium test. Using the heats of fusion for aluminum and cadmium given by Holsapple,[3] the simulated impact velocity is $U_{Al} = 3.1U_{Cd}$. Cadmium is unique among all metals in that it satisfies the requisite similarity conditions[3,4] (e.g., impactor momentum) and provides the velocity scale factor of 3.1. For this reason, cadmium experiments at actual velocities of 2 to 7 km/s can be used to simulate aluminum-on-aluminum impacts over a velocity range of about 7 to 21 km/s.

The third term on the right side of Eq. (1) is referred to as a nondimensional geometry parameter, in the sense that it involves the three geometry variables: bumper thickness, spacing, and wall thickness. (The term "geometry" might also be construed to indicate the shape or orientation of the bumper or wall. However, because this analysis is concerned only with Whipple shields, it is implicitly understood that the bumper and wall are represented by parallel flat plates of effectively infinite lateral extent.) For convenience, the nondimensional geometry parameter is denoted by π_t.

Several models of the high-velocity response of Whipple shields have been reported in the literature. For example, Maiden et al.[6] and Gehring[7] described an expression for d under an "optimum" condition in which the debris cloud contains only molten and vaporized material and therefore presents a blast loading to the wall. For fixed impactor, bumper, and wall materials, their result is

$$\frac{d}{b} \propto \left(\frac{tS^2}{b^3}\right)^{\frac{1}{3}} U^{-\frac{1}{3}} \tag{2}$$

Madden[8] developed a comparable relationship, except that the exponents were $\frac{1}{4}$ and $-\frac{1}{4}$, rather than $\frac{1}{3}$ and $-\frac{1}{3}$. Cour-Palais[9] constructed an empirical relation for a "nonoptimum" case, in which solid fragments are present in the debris cloud:

$$\frac{d}{b} \propto \left(\frac{t^2S}{b^2}\right)^{\frac{1}{2}} U^{-1} \tag{3}$$

This result was later modified by Christiansen[10,11] according to impact tests at velocities near 7 km/s. For constant impact angle and material types his model gives

$$\frac{d}{b} \propto \left(\frac{t^2S}{b^3}\right)^{\frac{1}{3}} U^{-\frac{2}{3}} \tag{4}$$

Equation (1) is comparable to Eqs. (2–4) in the sense that d/b depends on t, S, and b only through a single parameter. In the case of Eq. (2), that parameter is π_t. On the other hand, Eqs. (3) and (4) involve a different form of the geometry parameter. Additionally, note that Eqs. (2–4) all imply that d is independent of bumper thickness and varies as a power of the impact velocity. In contrast, Eq. (1) allows an arbitrary dependence on the bumper thickness and impact velocity. Differences such as these have resulted in significant uncertainty in the estimated performance of Whipple shields at high impact velocities.

This paper presents a summary of experiments performed to assess the validity of Eq. (1) and to discriminate among the various scaling relationships shown above. In particular, three questions are addressed:

1) Is the response of a Whipple shield characterized by the single nondimensional geometry parameter π_t, or some other parameter, such as appears in Eqs. (3) and (4)?

2) How does the normalized impactor diameter d/b depend on the geometry parameter?

3) For a given geometry, how does d/b depend on the impact velocity for simulated velocities above 7 km/s?

In addition to addressing these questions, the results are used to construct an empirical model for Whipple shields that gives the threshold impactor diameter for wall perforation.

Description of Experiments

The present tests were conducted at the University of Dayton Research Institute. A description of the facility is given in Ref. 12. Table 1 summarizes the initial conditions and results. In each test, a cadmium impactor struck a cadmium bumper at normal incidence. The walls were 2219-T87 aluminum sheets supported at each corner. As noted in Table 1, some of the experiments included multilayer insulation (MLI) placed midway between the bumper and the wall. The MLI, which consisted of layers (see Table 1) of 6-μm-thick sheets of aluminized Kapton, was included to facilitate comparisons with experiments reported in Ref. 13 for double-bumper shields. Three or four sets of orthogonal x-ray images were obtained for each test: one that verified the sphericity and integrity of the projectile prior to striking the bumper, and two or three images of the subsequent cloud growth and interaction with the wall. After a test, the diameter of the hole produced in the bumper was measured. Failure (i.e., perforation) of the wall was noted by visual inspection or, if questionable, by the passage of alcohol poured into the bulge in the wall. For tests that did not result in significant perforation or petaling of the wall, the maximum depth of the bulge was measured and is reported in Table 1.

Scaling Tests

To determine the validity of Eq. (1) a series of tests were performed at fixed values of the scaled velocity, angle, and tS^2/b^3, but at differing values of the individual parameters t, S, and b. If Eq. (1) is correct, these tests will give a common value of d/b for the ballistic limit (i.e., the threshold for wall perforation), because the right-hand side of the equation is constant. On the other hand, the tests will give differing values of d/b if Eq. (1) has omitted any additional dependence on spacing or wall thickness, or if the geometry parameter has the form shown in Eq. (3) or (4).

Table 1 Summary of experimental results[a]

Shot number	Impactor mass m, g	Impactor diameter d, mm	Impactor velocity V, km/s	Scaled velocity U, km/s	Bumper thickness b, mm	MLI no. sheets	Bumper spacing S, mm	Wall thickness t, mm	Wall size, mm × mm	Wall failed?	Bumper hole diam, mm	Wall bulge, mm	Geometry parameter $\pi_t = tS^2/b^3$	d/b
4-1648c	1.168	6.36	5.15	15.97	2.21	None	73	3.18	254 × 254	Yes	20.3	—	1.59E+03	2.88
4-1666c	3.768	9.40	5.57	17.27	1.27	None	144	3.18	406 × 406	Yes	19.6	—	3.20E+04	7.40
4-1667c	1.883	7.46	5.50	17.05	1.27	None	144	1.60	406 × 406	Yes	17.0	—	1.61E+04	5.88
4-1668c	2.758	8.47	5.68	17.61	1.27	None	144	3.18	406 × 406	No	19.1	35.5	3.20E+04	6.67
4-1669c	1.424	6.80	5.65	17.52	1.27	None	144	1.60	406 × 406	No	16.5	36.6	1.61E+04	5.35
4-1672c	2.227	7.89	5.77	17.89	2.11	21	110	3.18	337 × 406	No	25.2	26.4	4.10E+03	3.74
4-1674c	0.294	4.02	5.60	17.36	1.27	None	51	1.59	406 × 406	Yes	12.9	—	2.00E+03	3.16
4-1675c	0.245	3.78	5.70	17.67	1.27	None	51	1.59	406 × 406	No	12.4	9.4	2.00E+03	2.98
4-1676c	0.094	2.75	3.29	10.20	1.27	None	51	1.59	406 × 406	No	8.2	1.0	2.00E+03	2.16
4-1678c	0.196	3.51	3.43	10.63	1.27	None	51	1.59	406 × 406	No	10.2	3.2	2.00E+03	2.76
4-1679c	0.291	4.00	3.46	10.73	1.27	None	51	1.59	406 × 406	Yes	10.6	17.5	2.00E+03	3.15
4-1688	1.675	7.09	5.14	15.93	3.18	14	73	3.18	254 × 254	No	27.6	23.1	5.35E+02	2.23
4-1689	2.038	7.66	5.16	16.00	3.18	14	73	3.18	254 × 254	No	28.7	32.6	5.35E+02	2.41
4-1690	1.244	6.50	3.49	10.82	3.18	14	73	3.18	254 × 254	No	22.4	8.9	5.35E=02	2.05
4-1691	1.703	7.22	3.37	10.45	3.18	14	73	3.18	254 × 254	No	23.5	13.8	5.35E+02	2.27
4-1692	2.267	7.94	5.27	16.34	3.18	14	73	3.18	254 × 254	Yes	30.1	—	5.35E+02	2.50
4-1693	2.022	7.64	3.35	10.39	3.18	14	73	3.18	254 × 254	Yes	24.5	—	5.35E+02	2.41
4-1694	0.850	5.72	5.28	16.37	2.21	14	73	3.18	254 × 254	No	20.9	6.3	1.59E+03	2.59
4-1695	0.857	5.74	5.21	16.15	1.07	14	73	3.18	254 × 254	Yes	—	18.5	1.41E+04	5.38
4-1696	0.679	5.31	3.41	10.57	1.27	None	51	1.59	406 × 406	Yes	12.6	—	2.00E+03	4.41
4-1697	0.642	5.21	3.34	10.35	1.27	None	144	1.59	406 × 406	No	13.2	2.7	1.60E+04	4.10
4-1698	0.913	5.86	3.33	10.32	1.27	None	144	1.59	406 × 406	No	13.1	6.5	1.60E+04	4.62
4-1699	3.019	8.73	2.30	7.13	3.18	14	73	3.18	254 × 254	Yes	21.3	—	5.35E+02	2.75
4-1700	1.176	6.38	3.27	10.14	1.27	None	144	1.59	406 × 406	Yes	13.3	—	1.60E+04	5.02
4-1701	0.918	5.87	3.35	10.39	1.27	None	102	3.18	406 × 406	No	13.8	7.0	1.60E+04	4.63
4-1702	0.806	5.62	3.5	10.85	1.27	None	102	3.18	406 × 406	Yes	12.7	6.1	1.60E+04	4.43
4-1703	1.762	7.30	3.49	10.82	1.27	None	144	3.18	406 × 406	Yes	14.6	12.7	3.20E+04	5.75
4-1704	1.721	7.24	2.33	7.22	3.18	14	73	3.18	254 × 254	No	18.7	9.1	5.35E+02	2.28
4-1705	0.828	5.68	3.4	10.54	0.86	None	144	3.18	406 × 406	No	10.9	3.3	1.02E+05	6.57
4-1706	1.913	7.50	5.68	17.61	0.86	None	144	3.18	406 × 406	No	13.7	25.4	1.02E+05	8.69
4-1707	0.999	6.04	3.38	10.48	0.86	None	144	3.18	406 × 406	No	10.6	5.3	1.02E+05	7.00
4-1708	2.438	8.13	5.64	17.48	0.86	None	144	3.18	406 × 406	Yes	14.7	50	1.02E+05	9.42

[a]All shots were conducted at normal incidence with cadmium impactors and bumpers and 2219-T87 aluminum walls.

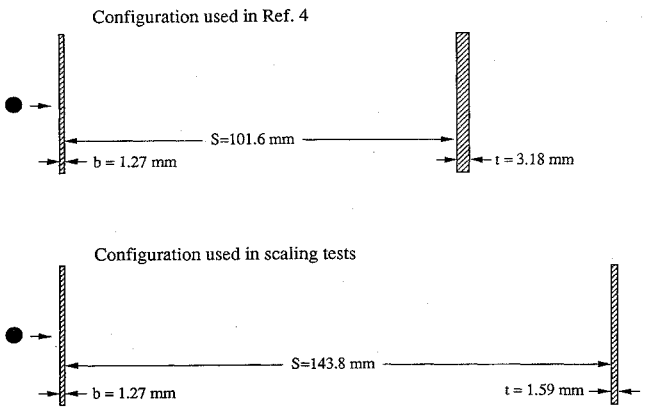

Fig. 2 Configurations used to test the scaling relationship given in Eq. (1).

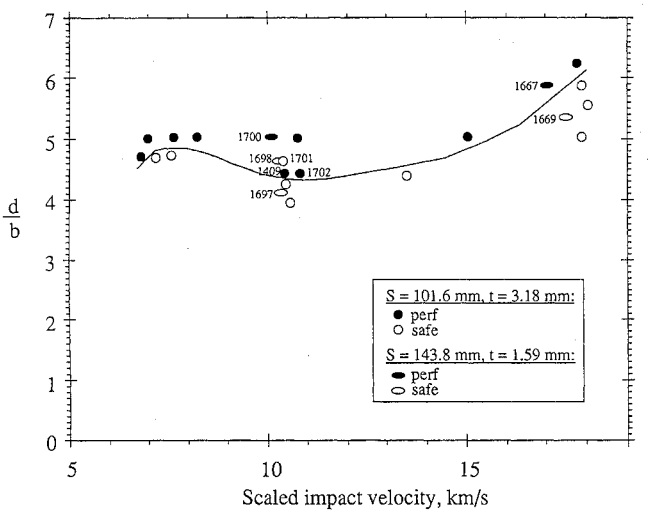

Fig. 3 Results of tests using the two configurations shown in Fig. 2.

A subset of the experiments reported in Ref. 4 was chosen as the baseline to be modeled. As shown in Fig. 2, those tests used fixed values of the bumper thickness, spacing, and wall thickness, and therefore a constant value of $\pi_t = tS^2/b^3 = 1.6 \times 10^4$. In the present study, tests were conducted with the wall thickness reduced by a factor of 2 and the spacing increased by a factor of $\sqrt{2}$ relative to the values used in Ref. 4 (see Fig. 2). Consequently, the present tests replicated the value of π_t used in Ref. 4 and, if Eq. (1) is correct, should agree with those results.

Figure 3 shows the data and a ballistic limit curve from Ref. 4 along with results from the present experiments. With the exception of shot 1409, all data points labeled with a shot number are from the present study. In particular, note that shots 1667 and 1669, which both used the relatively thin wall and large spacing, agree with the baseline results. That is, 1667, which perforated, is above the baseline ballistic limit curve, and shot 1669, which did not perforate, is below the curve. Therefore, for a scaled velocity near 17 km/s, Eq. (1) correctly accounts for the differing configurations of the two shield systems shown in Fig. 2.

Tests conducted at a scaled velocity of about 10.5 km/s also agreed with the baseline data, but showed a curious effect. While shots 1697 and 1700, which both used the thin wall and large spacing, straddled the curve shown in Fig. 3, shot 1698 did not perforate, even though it used a larger impactor than shot 1409, a baseline shot that showed a pinhole perforation. Shot 1701, which used the baseline spacing and wall thickness at the same impactor diameter as 1698, also did not perforate. It was suspected that shot 1409 was anomalous. However, shot 1702, a repeat of 1409, reproduced the pinhole perforation observed in 1409, suggesting that the ballistic limit is double-valued in the vicinity of these data points.

It is also possible, though unlikely, that shot 1701 is anomalous. If 1701 were discarded, then the fact that shot 1698 did not perforate while 1409 and 1702 did would imply a discrepancy of 4.3% in impactor diameter between the two shield configurations (i.e., $d_{1698}/d_{1702} = 5.86/5.62 = 1.043$). We believe this to be an unlikely hypothesis, considering the excellent reproducibility demonstrated by the University of Dayton facility. Three reproducibility tests were conducted between the present test series and our earlier tests.[4] For example, shots 1411 and 1422 (see Ref. 4) used cadmium impactors with $d = 5.98$ and 5.95 mm, and simulated impact velocities of 7.6 and 7.2 km/s, respectively, and neither perforated the wall; they left nearly equal bulge depths of 5.3 and 4.8 mm. Likewise, shots 1416 and 1417 used aluminum impactors and bumpers with $d = 5.96$ mm, and impact velocities of 7.09 and 6.94 km/s. Again, neither shot perforated, and both produced a bulge of depth 2.0 mm. Finally, as noted above, shot 1702 of the present series reproduced the pinhole perforation exhibited by shot 1409. Based on these tests, and the fact that shot 1701 exhibited no apparent faults (e.g., deformation or damage to the impactor prior to striking the bumper), shot 1701 is believed to be a valid test. In either case, the agreement between the model-of-model tests at both 17 and 10.5 km/s indicates that Eq. (1) provides a good description of the effect of t, S, and b on the ballistic limit for impacts of spherical particles on single-bumper shields.

Effects of Geometry on Shield Performance

The tests discussed in the previous section were conducted at a value of $\pi_t = 1.6 \times 10^4$. Additional tests were performed with $\pi_t = 535$, 2000, 3.2×10^4, and 10^5 to determine how the ballistic limit depends on this geometry parameter. Figure 4a shows the results as impactor diameter versus simulated velocity (i.e., 3.1 U_{Cd}). The shape of the ballistic limit curve is seen to depend on the geometry of the dual-wall system. For example, the results for $b = 3.18$ mm, $S = 73.4$ mm, $t = 3.18$ mm show a curve that is nearly flat for velocities above 11 km/s, whereas the curve for $b = 1.27$ mm, $S = 143.8$ mm, $t = 3.18$ mm shows a marked increase with velocity.

It is not clear from Fig. 4a why some of the curves are flat, while others slope upward for simulated velocities above about 11 km/s. However, as shown in Fig. 4b, normalizing the impactor diameter by the bumper thickness, i.e., plotting in the form consistent with Eq. (1), reveals a consistent trend in the data. The experiments with the smaller values of π_t (535 and 2000) have ballistic limit curves that are nearly flat, while the curves for larger values of π_t slope upward at high velocities.

In agreement with the findings of Hopkins et al.,[5] Ref. 4 concluded from tests at $\pi_t = 1.6 \times 10^4$ that the upward trend in the ballistic limit curve above 11 km/s is due to the effects of vaporization of the impactor and bumper. Aluminum begins to vaporize on unloading at an impact velocity of 10.9 km/s (see Ref. 3). For somewhat slower impacts, the debris cloud consists primarily of melted material. As the impact velocity increases, much of the melted material is replaced by vapor, thereby smearing out the concentrated loadings that would have been presented by melt droplets. Hence, as velocity increases, the loading on the wall becomes less lethal, and the ballistic limit increases. This mechanism explains the upward-sloping curves for velocities above 11 km/s; but why are the curves for $\pi_t = 535$ and 2000 relatively flat?

To answer this question, note that the two flat curves in Fig. 4b not only correspond to the smallest values of π_t, but also to the smallest values of d/b, as illustrated by the drawings of impactor and bumpers on the left side of the figure. When d/b is large, an incremental increase in velocity vaporizes additional impactor material, so the ballistic limit curve goes up, as discussed above. On the other hand, when d/b is small, an increase in velocity may not result in significantly more vaporization, because most of the impactor material is already vaporized. That is, impacts with small d/b do not have the reservoir of material to vaporize that large-d/b impacts have. Hence, the ballistic limit curve is relatively flat if d/b is small, viz., less than about 3, according to Fig. 4b.

Therefore, the shape of the ballistic limit curve depends on the geometrical configuration of a dual-wall system. For example, consider a system that has $\pi_t = 1000$. According to Fig. 4b, the ballistic limit curve for this case will be nearly flat for velocities above 7 km/s. Now suppose the bumper spacing is increased by a factor of 4, so that $\pi_t = 1.6 \times 10^4$. The increase in spacing means that larger projectiles are required to perforate the wall, i.e., the values of d/b increase. Consequently, not only does the ballistic limit curve shift up, but its shape changes to one with a positive slope for velocities above about 11 km/s, thus providing a dramatic improvement in shield performance at high velocities.

Figure 5 shows d/b as a function of π_t for simulated velocities of 10.5 km/s and 17.5 km/s. The five data points denoted with an asterisk (*) at the end of their shot name had the impactor diameter "corrected" to account for the fact that not all of the high-velocity shots were conducted at a simulated velocity of exactly 17.5 km/s. The slight adjustment was accomplished by moving them to a velocity of 17.5 km/s along a line parallel to the ballistic limit curve shown in Fig. 4b. The adjustment in d was typically a few percent, except for shot 1695, whose diameter was increased by 11%. None of the points for 10.5 km/s were adjusted, because all of the ballistic limit curves are insensitive to variations in velocity between 10 and 11 km/s. Figure 5 shows that, for π_t less than a few thousand, the 17.5-km/s curve is quite close to the curve for 10.5 km/s. This is consistent with the above observation that the ballistic limit curves for $\pi_t = 535$ and 2000 are nearly independent of velocity. For π_t greater than a few thousand, the 17.5-km/s curve lies significantly above the lower-velocity results, reflecting the upward-sloping curves shown in Fig. 4b for large π_t.

Note that the axes in Fig. 5 are logarithmic, so that a straight line indicates a power-law relationship between d/b and π_t. In this case, Eq. (1) becomes

$$\frac{d}{b} = \left(\frac{tS^2}{b^3}\right)^{\phi} f\left(\frac{U}{\sqrt{h_i}}, \theta\right) \tag{5}$$

where ϕ is an exponent to be determined. Therefore, $d \propto b^{1-3\phi}$ when all other variables are held constant. Hence, as b increases, d increases, remains constant, or decreases for the three cases of $\phi < \frac{1}{3}$, $\phi = \frac{1}{3}$, or $\phi > \frac{1}{3}$. The results shown in Fig. 5 indicate that ϕ is generally less than $\frac{1}{3}$, so that increases in bumper thickness should improve shield performance. The portion of the 17.5-km/s curve between $\pi_t = 2000$ and 10^4 is consistent with $\phi = \frac{1}{3}$. At this velocity, and over this limited range, the ballistic limit is insensitive to bumper thickness. However, it has been noted from aluminum experiments at velocities below about 7 km/s that increases in bumper thickness do not always result in an increase in shield performance.[9] Therefore, the trends shown in Fig. 5 may not apply to that lower velocity range. To summarize, for velocities greater than 7 km/s, increases in bumper thickness should improve, or at least not degrade, shield performance.

Comparison with Previous Results

As noted in the Introduction, scaling equations for high impact velocities have been developed in previous studies. For example, the relationship presented by Gehring[7] and shown above in Eq. (2) is a special case of Eq. (5) in which $\phi = \frac{1}{3}$ and the velocity function f is a power law in its argument. Equation (2) is partially consistent with the present results in the sense that the shield configuration is specified through π_t alone. However, the dependence on π_t in Eq. (2) is inconsistent with the results shown in Fig. 5. That is, although the data in Fig. 5 can be described by a sequence of connected power-law segments, the exponent ϕ is not constant and generally differs from $\frac{1}{3}$. Additionally, the monotonic power-law velocity dependence in Eq. (2) does not agree with the more complicated dependence shown by the results in Fig. 4b for simulated velocities between 7 and 18 km/s.

The "nonoptimum" relation of Cour-Palais[9] shown in Eq. (3) can be rewritten in terms of π_t as

$$\frac{d}{b} \propto \pi_t \frac{b^2}{S^{\frac{3}{2}}} U^{-1} \tag{6}$$

If Eq. (6) correctly described the dependence on wall thickness and bumper spacing, then the scaling tests described above would have

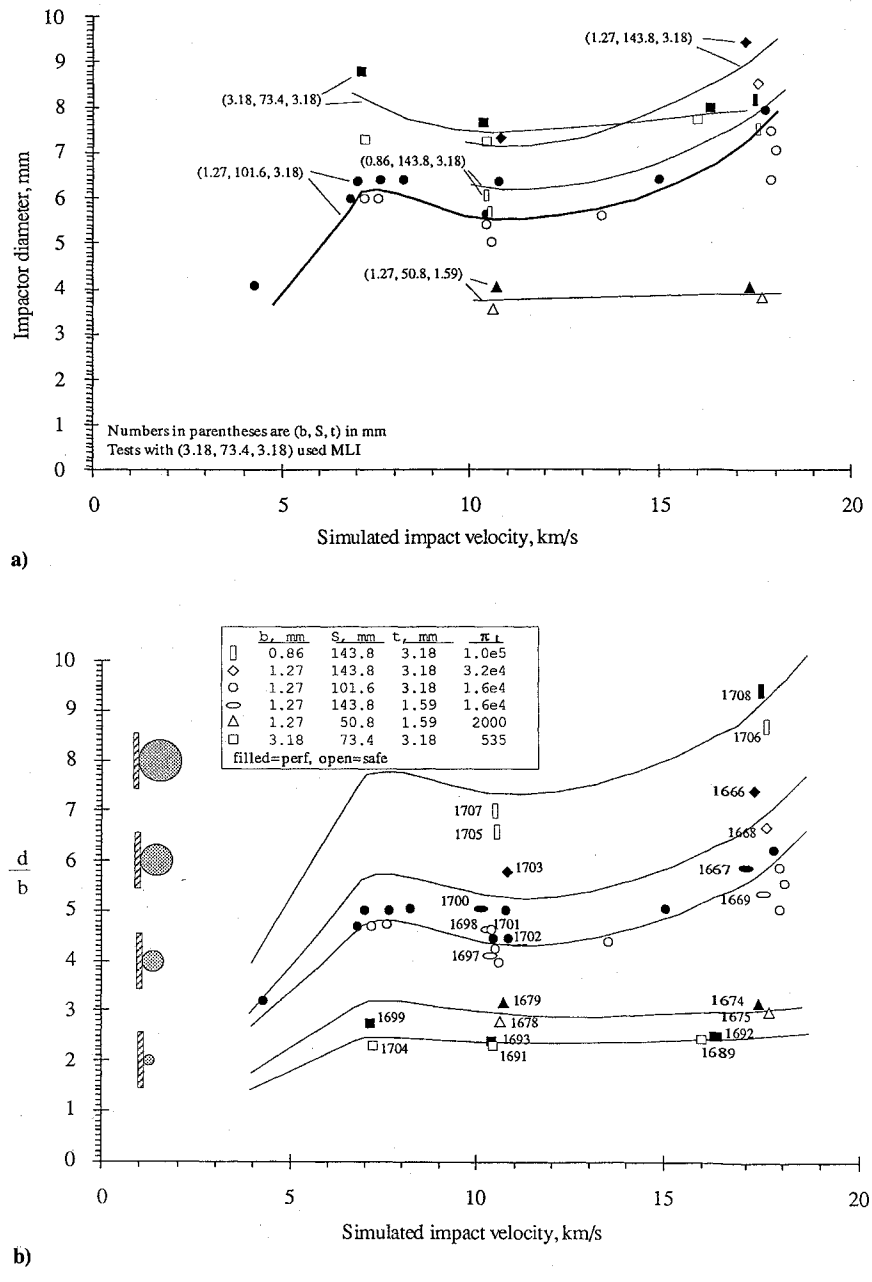

Fig. 4 a) Ballistic limit results for five different Whipple shield configurations and b) impactor diameter normalized by bumper thickness.

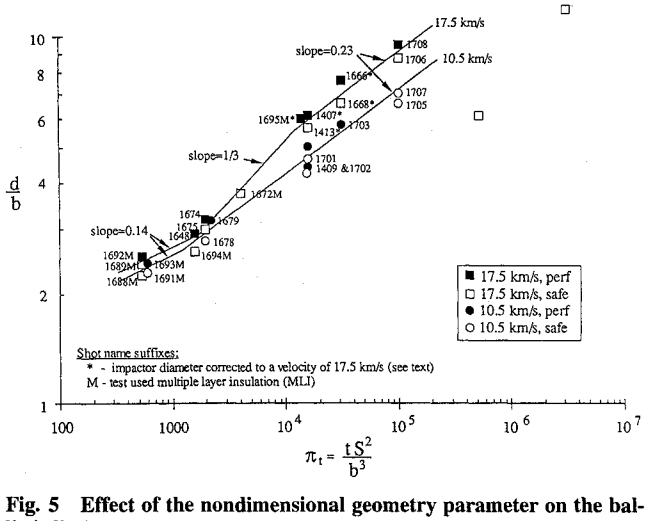

Fig. 5 Effect of the nondimensional geometry parameter on the ballistic limit.

given markedly different values of the threshold impactor diameter for perforation. Recall that those tests used constant values of U, b, and π_t, but differing values of t and S. In particular, S was varied by a factor of 1.4. Therefore, according to Eq. (6), the small-spacing tests shown in Fig. 3 should have exhibited a value of d that was 1.7 times larger than the value found for the large-spacing tests. In contrast, the results in Fig. 3 show that d does not vary by more than about 10% between the two configurations.

Similar comments apply to the scaling equation given in Refs. 10 and 11. That equation, given above as Eq. (4), can be rewritten as

$$\frac{d}{b} \propto \pi_t^{\frac{2}{3}} \frac{b}{S} U^{-\frac{2}{3}} \tag{7}$$

This equation indicates that a factor-of-1.4 variation in d should have occurred in the scaling tests, contrary to the actual observations. In summary, the t and S dependences given in Eqs. (6) and (7), or equivalently in Eqs. (3) and (4), are inconsistent with the results of the scaling tests for the simulated velocities considered.

A Prediction Equation

An empirical model was constructed to allow the results of cadmium simulations to be used in calculating ballistic limit curves for a single-bumper shield having a 2219-T87 aluminum wall (the material used in Ref. 4 and in the present study). A function was chosen that consists of a linear combination of a constant term, a "Gaussian bump" (which models the observed peak in the ballistic limit curve near 7 km/s), and an exponential term (which emulates the observed behavior for velocities above about 11 km/s):

$$\frac{d}{b} = A + B\exp[-0.17(U\cos\theta - 7.5)^2] + C\exp[0.3U\cos\theta] \quad (8)$$

where θ is the angle of impact on the bumper, measured from the normal. For convenience, and in the absence of definitive tests, the dependence on angle is assumed to be of the form $U\cos\theta$, i.e., it is assumed that an impact event is described by the normal component of the velocity. Although this assumption needs to be confirmed through further simulations, partial support is found from shots 1439 and 1440 reported in Ref. 4. Those tests were conducted at an impact angle of 54 deg from the normal and a simulated velocity of 17.5 km/s, giving a normal component velocity of 10.2 km/s. Both shots perforated, in agreement with tests conducted at normal angle of incidence at a simulated velocity near 10 km/s.

The parameters A, B, and C depend on π_t and were fitted to the data to obtain

$$A(\pi_t) = \begin{cases} 0.87\pi_t^{0.157}, & \pi_t \le 1.6\times 10^4 \\ 0.218\pi_t^{0.3}, & \pi_t > 1.6\times 10^4 \end{cases} \quad (9)$$

$$B(\pi_t) = \begin{cases} 0.003\pi_t^{0.624}, & \pi_t \le 7000 \\ 0.75, & \pi_t > 7000 \end{cases} \quad (10)$$

$$C(\pi_t) = \begin{cases} 0.001, & \pi_t \le 2000 \\ 2.17\times 10^{-7}\pi_t^{1.11}, & 2000 \le \pi_t \le 1.6\times 10^4 \\ 3.8\times 10^{-3}\pi_t^{0.1}, & \pi_t > 1.6\times 10^4 \end{cases} \quad (11)$$

Equations (8–11) were used to construct the curves shown in Fig. 4b for velocities above 7 km/s. As can be seen in that figure, the empirical model provides a good fit to the cadmium results. However, it is emphasized that because this is an empirical fit, it should only be used over the range of scaled velocity and π_t covered by the results, i.e., 7 km/s $< U <$ 18 km/s, *and* $500 < \pi_t < 10^5$.

Equation (8) applies only for normal velocities above 7 km/s. For normal-component velocities below 3 km/s, the relationship given in Refs. 10 and 11 is adopted. Using the material parameters for 2219-T87 aluminum, that model gives, for $U\cos\theta < 3$ km/s,

$$\frac{d}{b} = \frac{1}{b}\left(\frac{1.14t + b}{\cos^{\frac{5}{3}}\theta U^{\frac{2}{3}}}\right)^{\frac{18}{19}} \quad (12)$$

In Ref. 10, an expression for intermediate impact velocities was obtained by linearly interpolating in velocity between the low-velocity and high-velocity relationships. Using a similar procedure, a linear interpolation between Eq. (8) and Eq. (12) gives, for 3 km/s $< U\cos\theta <$ 7 km/s,

$$\frac{d}{b} = \left(\frac{7 - U\cos\theta}{4}\right)\frac{0.5}{b}\left(\frac{1.14t + b}{\cos\theta}\right)^{\frac{18}{19}} + \frac{U\cos\theta - 3}{4}(A + 0.958B + 8.17C) \quad (13)$$

Equations (8), (12), and (13) determine the ballistic limit for all velocities up to 18 km/s and provide a guide that can be used to design single-bumper shields.

In Figs. 6–8 test results are compared with ballistic limit curves calculated from the above equations. Each figure presents a family of curves corresponding to a range of values of one of the variables b, S, or t, while the other two are held constant. The particular cases shown in the figures were chosen to provide a comparison

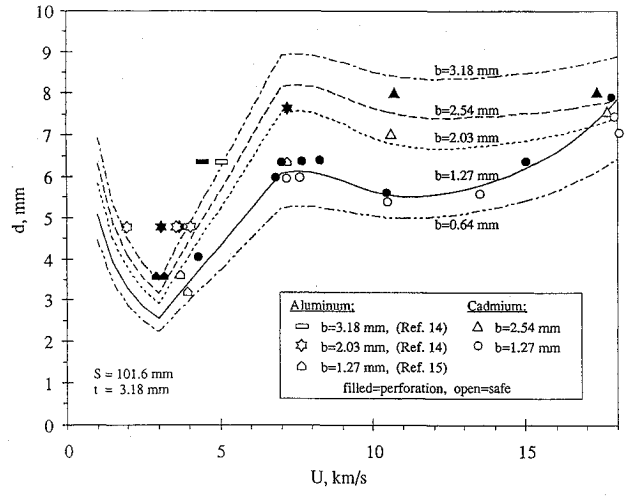

Fig. 6 Comparison of Eqs. (8–13) with test data illustrating the effect of varying bumper thickness at fixed wall thickness and bumper spacing.

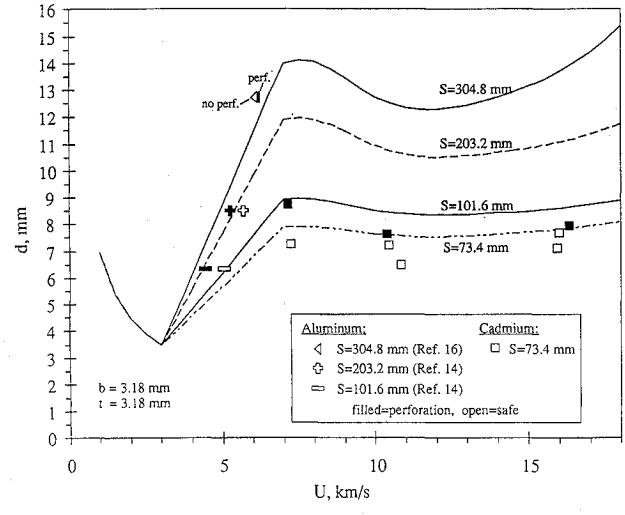

Fig. 7 Comparison of Eqs. (8–13) with test data illustrating the effect of varying bumper spacing at fixed wall thickness and bumper thickness.

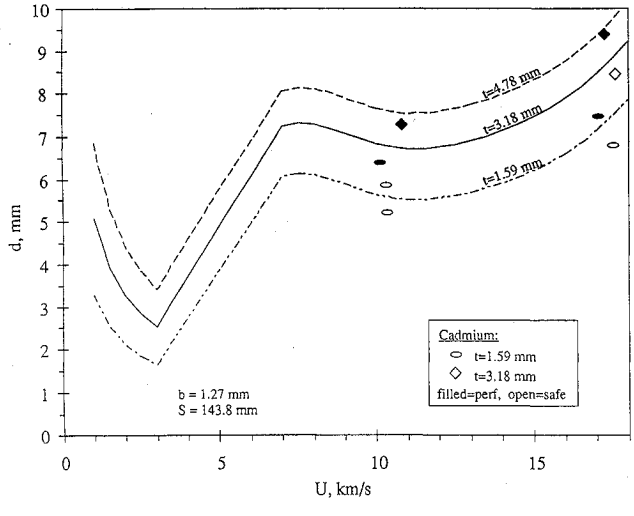

Fig. 8 Comparison of Eqs. (8–13) with test data illustrating the effect of varying wall thickness at fixed bumper spacing and thickness.

with the largest subset of test data available for 2219-T87 walls. Figure 6 corresponds to normal impacts on a shield with a spacing $S = 101.6$ mm and a wall thickness $t = 3.18$ mm. Curves are shown for five values of the bumper thickness. An examination of this figure shows that the calculated curves correctly fit all of the test results except for $b = 2.03$ mm and $b = 1.27$ mm at velocities between 3 and 5 km/s, for which the curves somewhat

underestimate the threshold diameter for perforation. Figure 7 shows the effect of variations in bumper spacing at a fixed bumper thickness (3.18 mm) and wall thickness (3.18 mm). Again, the curves provide a reasonable fit to the available data. Figure 8 shows computed curves for three values of the wall thickness for fixed bumper thickness of $b = 1.27$ mm and spacing $S = 143.8$ mm. Note that the computed curve for $t = 1.59$ mm passes below a data point for a nonperforation near 10.5 km/s. This is due to the fact that, as discussed above, the ballistic limit may be double-valued in this region; the curve was constructed to pass below the smallest perforation event (see Fig. 3).

Conclusions

Cadmium simulations of high-velocity aluminum impacts were performed in order to test the validity of a scaling relationship for the minimum-size impactor able to perforate a wall protected by a single-bumper debris shield. According to the scaling relationship, the bumper thickness, spacing, and wall thickness are described through a single nondimensional parameter. Tests were conducted at simulated aluminum impact velocities near 11 and 17 km/s using two shield configurations that should behave identically because they had a common value of the nondimensional parameter. The observed agreement in these tests illustrates that for velocities above 7 km/s the effects of bumper thickness, spacing, and wall thickness are correctly accounted for by the single parameter.

For single-bumper shields, the shape of the ballistic limit curve, which gives the threshold impactor diameter for wall perforation as a function of velocity, was shown to depend on the value of the nondimensional parameter. When the parameter is small, the curve is quite flat for simulated velocities above about 10 km/s. That is, the threshold particle size for perforation is insensitive to impact velocity. On the other hand, for larger values of the parameter, the threshold impactor size increases markedly as the velocity increases. This is believed to be due to increased vaporization of the impactor and bumper material at high velocities.

An empirical model was constructed, based on cadmium simulations for normal-component velocities above 7 km/s and on an existing model for normal-component velocities below 3 km/s. The resulting ballistic limit equations provide a good description of available test data for experiments using 2219-T87 aluminum walls.

Acknowledgments

This research was supported by Boeing Defense and Space Group Independent Research and Development funds. We greatly appreciate the diligent efforts of K. Poormon and A. Piekutowski in performing the experiments and useful comments from M. Bjorkman, K. Holsapple, and two anonymous reviewers.

References

[1]Westine, P. S., and Mullin, S. A., "Scale Modeling of Hypervelocity Impact," *International Journal of Impact Engineering*, Vol. 5, Nos. 1–4, 1987, pp. 693–701.

[2]Mullin, S. A., Anderson, C. E., Jr., and Wilbeck, J. S., "Dissimilar Material Scaling Relationships for Hypervelocity Impact," Defense Nuclear Agency, DNA-TR-89-112, Washington, DC, July 1989.

[3]Holsapple, K. A., "Hypervelocity Impacts: Testing in Surrogate Materials," *International Journal of Impact Engineering*, Vol. 14, Nos. 1–4, 1993, pp. 335–345.

[4]Schmidt, R. M., Housen, K. R., Piekutowski, A. J., and Poormon, K. L., "Cadmium Simulation of Orbital Debris Shield Performance to Scaled Velocities of 18 km/s," *Journal of Spacecraft and Rockets*, Vol. 31, No. 5, 1994, pp. 866–877.

[5]Hopkins, A. K., Lee, T. W., and Swift, H. F., "Material Phase Transformation Effects upon the Performance of Spaced Bumper Systems," *Journal of Spacecraft and Rockets*, Vol. 9, No. 5, 1972, pp. 342–345.

[6]Maiden, C. J., Gehring, J. W., McMillan, A. R., and Sennett, R. E., "Experimental Investigations of Simulated Meteoroid Damage to Various Spacecraft Structures," NASA TR 65-48, 1965.

[7]Gehring, J. W., "Theory of Impact on Thin Targets and Shields and Correlation with Experiment," *High Velocity Impact Phenomena*, 1st ed., edited by R. Kinslow, Academic, New York, 1970, pp. 105–156.

[8]Madden, R., "Ballistic Limit of Double-Walled Meteoroid Bumper Systems," NASA TN, D-3916, April 1967.

[9]Cour-Palais, B. G., "Meteoroid Protection by Multi-wall Structures," AIAA Paper 69-372, May 1969.

[10]Christiansen, E. L., "Whipple Shield Sizing Equations," NASA TM-105539, March 1991.

[11]Christiansen, E. L., "Design and Performance Equations for Advanced Meteoroid and Debris Shields," *International Journal of Impact Engineering*, Vol. 14, Nos. 1–4, 1993, pp. 145–156.

[12]Piekutowski, A. J., "Debris Clouds Generated by Hypervelocity Impact of Cylindrical Projectiles with Thin Aluminum Plates," *International Journal of Impact Engineering*, Vol. 5, Nos. 1–4, 1987, pp. 509–518.

[13]Schmidt, R. M., Housen, K. R., and Ahlstrom, H. G., "Experiments and Analysis of Orbital Debris Shock Penetration of Pressure Vessels in Space," *Proceedings of the 19th International Symposium on Shock Waves* (Marseille, France), Springer-Verlag (to be published).

[14]Williams, D. R., and Bjorkman, M. D., "Results of Ballistic Limit Testing of Aluminum Meteoroid/Debris Shields," Boeing Defence and Space Group, Document D683-10578-1, Contract NAS8-50000, Seattle, WA, 1992.

[15]Christiansen, E. L., "Whipple, Multi-Shock, and Mesh Double-Bumper Shield Hypervelocity Impact data," NASA JSC Memorandum SN3-91-95, June 1991.

[16]Schonberg, W. P., and Bean, A. J., "Hypervelocity Impact Response of Aluminum Multi-Wall Structures," *Acta Astronautica*, Vol. 25, No. 7, 1991, pp. 363–373.